

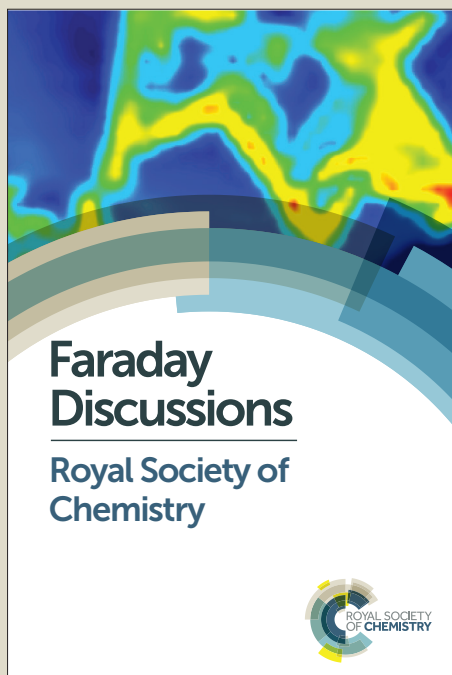
Faraday Discussions

Accepted Manuscript



This manuscript will be presented and discussed at a forthcoming Faraday Discussion meeting. All delegates can contribute to the discussion which will be included in the final volume.

Register now to attend! Full details of all upcoming meetings: <http://rsc.li/fd-upcoming-meetings>



This is an *Accepted Manuscript*, which has been through the Royal Society of Chemistry peer review process and has been accepted for publication.

Accepted Manuscripts are published online shortly after acceptance, before technical editing, formatting and proof reading. Using this free service, authors can make their results available to the community, in citable form, before we publish the edited article. We will replace this *Accepted Manuscript* with the edited and formatted *Advance Article* as soon as it is available.

You can find more information about *Accepted Manuscripts* in the [Information for Authors](#).

Please note that technical editing may introduce minor changes to the text and/or graphics, which may alter content. The journal's standard [Terms & Conditions](#) and the [Ethical guidelines](#) still apply. In no event shall the Royal Society of Chemistry be held responsible for any errors or omissions in this *Accepted Manuscript* or any consequences arising from the use of any information it contains.

ARTICLE

Cite this: DOI: 10.1039/x0xx00000x

Received 00th January 2012,
Accepted 00th January 2012

DOI: 10.1039/x0xx00000x

www.rsc.org/

Highly efficient organic devices based on small-molecule organic semiconductors

V.G. Lyssenko,^a S. Hofmann^a and K. Leo^a

We discuss approaches to increase the light outcoupling efficiency in organic microcavity lasers (MCs) and organic light-emitting diodes (OLEDs). We find that the introduction of metals into cavities leads to additional Tamm-plasmon polariton modes, while the corrugation of metal contacts, like perforated μ -size holes or a periodic array of metal stripes leads to 2D confinement of the cavity modes, which in turn reduces the lasing threshold in MCs. Furthermore, we elucidate light loss mechanisms in OLEDs and reveal how external dielectric layers and periodic gratings can be used to enhance outcoupling from the OLED cavity.

Received (in XXX, XXX) Xth XXXXXXXXX 200X, Accepted Xth XXXXXXXXX 200X

First published on the web Xth XXXXXXXXX 200X

DOI: 10.1039/b000000000x

Introduction

In the past years, devices based on organic semiconductors have made rapid progress. To gain knowledge about interactions between light and matter, organic microcavities (MCs), i.e. an organic light-emitting material sandwiched between two dielectric mirrors (distributed Bragg reflectors, DBR), are widely studied. Especially, the introduction of metal layers is of interest to construct an electrically driven organic solid state laser and important progress has already been achieved.¹

First organic light-emitting devices (OLEDs) were demonstrated by Tang and VanSlyke in 1987.² Nowadays, OLEDs are widely used as display for smart phones or for lighting applications. In comparison to common light sources, OLEDs have several advantages: they are

flat area emitters offering a diffuse light perception, wide viewing angles, and can be realized on flexible substrates. For both display and lighting applications, high efficiency is crucial. The efficiencies reached with the first OLEDs were quite low. For optimization, an adequate understanding of electric, excitonic, and optical processes limiting efficiencies is required. The reason for the low efficiency are: (i) the inefficient injection and transport of charge carriers which is hindered by space-charge limited currents and contact resistance, (ii) the used fluorescent emitter system, i.e. all electrically excited triplets are a lost, and (iii) the light outcoupling is not optimized for this thin film structure, i.e. light is trapped inside the OLED.

Electrical improvements regarding charge injection from the contacts and charge carrier transport can be achieved by adding blocking layers and (molecularly) doped transport layers. With

ARTICLE

the latter, a pin-structure could be realized which has been intensively studied in the past years.³⁻⁷

Excitons are excited states that are responsible for light emission. They are generated by the recombination of holes and electrons, either forming a singlet or a triplet. Due to spin statistics, about 25% singlets and 75% triplets are generated in the OLED. Their distribution on the different emitter molecules is crucial for the design of efficient OLEDs. The internal quantum yield, i.e. the conversion efficiency of charge carriers into photons, in OLEDs comprising only phosphorescent emitters is nowadays almost 100%.

However, due to internal losses (total internal reflection, absorption, surface plasmon polaritons⁸), about 70 to 80% of the generated photons are trapped inside the OLED thin film structure and the substrate.⁹ Hence, optical properties and light outcoupling enhancement methods are the main remaining obstacles to achieve high efficiency¹⁰⁻¹⁴ of the OLEDs.

In the following, we cover the theoretical background of lasing in MCs. Furthermore, we investigate the introduction of metal layers and corrugation into the cavities and their influence on the lasing threshold. Finally, we elucidate light loss mechanisms in OLEDs and reveal how external dielectric layers and periodic gratings can be used to enhance the efficiency of top-emitting OLEDs.

Microcavities

In a planar microcavity¹⁵, photons are confined between DBRs in the cavity layer with thickness L_c and refractive index n_c . The emission of the excited cavity layer propagates in growth z -direction with resonance wavevector $k_z = \pi/n_c L_c$ and can propagate at an oblique angle φ with longitudinal wavevector k_x and a “parabolic-like” dispersion:

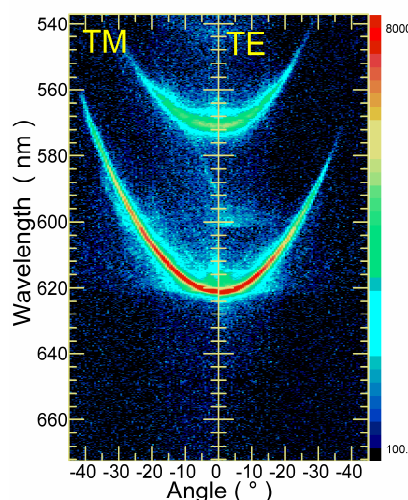


Fig. 1. Experimental angular-resolved TM- and TE-polarized emission spectra of the cavity parabola-like mode at 620 nm (see Eq. 1) and transmitted through DBR side-band at 570 nm.

This journal is © The Royal Society of Chemistry 2013

$$E(k_x) = \frac{\hbar c}{n_c} \sqrt{\left(\frac{\pi}{L_c}\right)^2 + k_x^2} \approx E(0) + \frac{\hbar^2 k_x^2}{2m_x}, \quad (1)$$

where $\pi\hbar c/n_c L_c = E(0)$ is the energy of the fundamental mode, $m_x = \pi\hbar n_c/cL_c$, while $k_x = \omega \sin\varphi/c$ is related to the angle φ of the emitted light. By measuring the angular-resolved reflection, transmission, or emission spectra of MCs, one can restore the true dispersion curves of exciton-polaritons and their nature. In Fig. 1, angular-resolved TE- and TM-polarized spontaneous emission spectra of the red fluorescent emitter 4-(dicyanomethylene)-2-methyl-6-[p-(dimethyl-amino)-styryl]-4H-pyran (DCM) doped into the matrix tris(8-hydroxy-quinolino)-aluminium (Alq_3), embedded between two DBRs and excited by a cw non-resonant 405 nm laser below lasing-threshold intensity, are shown. Both cavity-mode (620 nm) and emission through short-wavelength DBR sidebands (570 nm) show a parabolic-like dispersion according to Eq. (1).

Purcell Enhancement¹⁶. In 1946, Mills Purcell proposed to control the spontaneous emission (SE) rate of a monochromatic dipole with emitting wavelength λ_c and linewidth $\Delta\lambda_c$ by using a microcavity (MC) with a single cavity mode to tailor the number of electromagnetic modes to which it is coupled.¹⁷ For case of the “weak coupling” $\Delta\lambda_c \gg \Delta\lambda_e$, the escape time of SE photons out of the cavity is much shorter than the radiative lifetime and reabsorption is negligible. A simple derivation shows that the SE rate in the microcavity mode is given by the Purcell factor $F = 3Q\lambda_c^3 / 4\pi n^3 V$, where n is the refractive index of the medium and V is the effective mode volume. Additionally, the radiative rate Γ_r is strongly enhanced at above-threshold excitations, proportional to the density n of coherent photons. Therefore, the ratio $\Gamma_r / (\Gamma_r + \Gamma_{nr})$ can reach ~ 1 .

Rate Equations and Lasing¹⁸. Above threshold, lasing occurs when the round-trip gain is greater than the round-trip loss. The threshold is determined as the pump power at which the mean stimulated and spontaneous emission rates into the lasing mode are equal.¹⁹⁻²⁰ The rates of spontaneous emission into lasing and

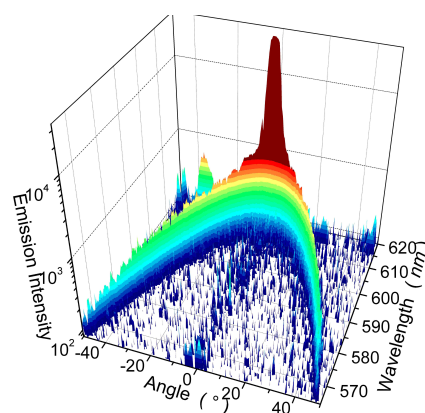


Fig. 2. Experimental angular-resolved emission above lasing threshold

J. Name., 2013, **00**, 1-3 | 2

ARTICLE

non-lasing modes are described as fractions, β and $1-\beta$, of the total spontaneous emission rate. Corresponding angular-resolved emission spectra at the above-threshold excitation is presented in Fig. 2. Due to the increased number of excited state molecules, both the gain and the rate of spontaneous emission Γ_{\perp} into non-lasing modes are increased.

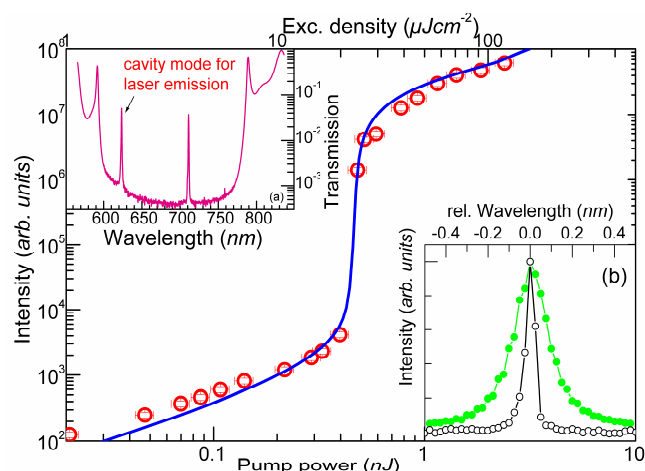


Fig. 3. Experimentally measured (circles) intensities of spontaneous and stimulated emission from organic MC and calculated using Eq. (5a).

The discussion of lasing in MC with a four-level homogeneously broadened gain medium can be carried out using rate equations.²¹ The model is defined by the Maxwell-Bloch equations:

$$\dot{\alpha} = -\kappa\alpha + g\nu, \quad (2a)$$

$$\dot{\nu} = -\gamma_{\perp}/2 + g\alpha N, \quad (2b)$$

$$\dot{N} = -\gamma_{\parallel}N + \Gamma + g(\alpha\nu^* + \nu\alpha^*), \quad (2c)$$

where α is complex amplitude of the laser field (in photon number units), N is a number of atoms in the upper level of the lasing transition, ν is the gain-medium polarization amplitude summed over all atoms, 2κ is the photon decay rate, γ_{\parallel} is the spontaneous emission rate to modes other than the laser mode, γ_{\perp} is full width at half maximum (FWHM) of the homogeneous gain, g is the dipole coupling constant, and Γ is excitation rate.

The polarization ν damps on a subpicosecond time scale may be therefore adiabatically eliminated. As a result, Eqs. (2) can be replaced by equivalent rate equations:

$$\dot{n} / \gamma_{\parallel} = -\lambda n + \beta n N, \quad (3a)$$

$$\dot{N} / \gamma_{\parallel} = -N + P - \beta n N, \quad (3b)$$

where $\lambda = 2\kappa/\gamma_{\perp}$, $P = \Gamma/\gamma_{\perp}$, $\beta = 4g^2/\gamma_{\perp}\gamma_{\parallel}$, and $n = |\alpha|^2$ is the photon number.

This journal is © The Royal Society of Chemistry 2013

Spontaneous emission into the laser mode can be included by the replacement of the photon number n by $n+1$ in the stimulated emission term $\beta n N$. Thus the generalized rate equations are:

$$\dot{n} / \gamma_{\parallel} = -\lambda n + \beta n N + \beta N, \quad (4a)$$

$$\dot{N} / \gamma_{\parallel} = -N + P - \beta n N - \beta N, \quad (4b)$$

where λ and P are cavity decay rate and pumping rate, respectively, measured in units of the spontaneous emission rate; β is the branching ratio which specifies the fraction of spontaneous emission directed into the laser mode. The steady-state solutions of Eqs. (4) are:

$$n = \frac{2P - \lambda \pm \sqrt{(2P - \lambda)^2 + 4\lambda\beta^2 P}}{2\lambda\beta}, \quad (5a)$$

$$N = P / (1 + \beta n), \quad \nu = 2g\alpha N / \gamma_{\perp}. \quad (5b)$$

Figure 3 presents experimentally measured (circles) intensities of spontaneous and stimulated emission from an organic MC and calculated using Eq. (5a). Here, experimental and calculated results are in remarkable agreement.

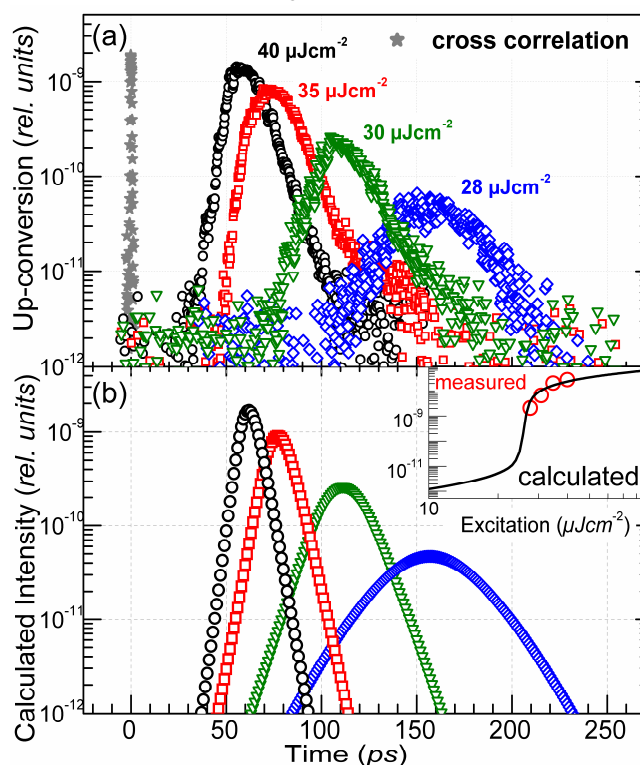


Fig. 4. (a) Time-resolved organic MC emission as measured by an up-conversion technique for pump powers above threshold. (b) The laser output is modeled by a set of rate equations for the different excitation energies²².

ARTICLE

In a next step, the temporal development of the emitted laser pulses above threshold is investigated in an up-conversion experiment, when the 800 nm pulse of the amplifier is split in two laser beams. One beam is frequency doubled and used as the ~400 nm pump beam of the organic MC. The MC emission is guided into another non-linear crystal and is added with the second 800 nm pulses, the gate beam, from the amplifier. Its temporal arrival can be varied by a delay stage in a range up to ~500 ps. The time resolution of this experiment is given by the gate pulse duration of about 200 fs. Figure 4 (a) presents five time traces of the organic laser for different pump powers above threshold. At the lowest recorded pump pulse power (0.78 nJ) the maximum output occurs about 150 ps after the arrival of the pump pulse with a pulse width of 60 ps. With increasing power, the MC pulse appears earlier and exhibits a narrower temporal width. After a nearly doubling of the excitation power to 1.3 nJ, the organic laser shows the highest output 40 ps after pump pulse incidence with a reduced width of 14 ps. The existence of the gain switched state is much shorter than the natural lifetime of the excited state as observed by the spontaneous emission lifetime. An additional requirement for gain switching is a short photon lifetime which is also fulfilled by $\tau_{\text{cav}} = 1.5$ ps. In our experiment, a 400 fs pump pulse excites a large number of Alq₃ molecules, which have a comparably long radiative lifetime of about $\tau_{\text{Alq}_3} = 20$ ns. The excitation is non-radiatively transferred to the DCM molecules with a lifetime of $\tau_{\text{DCM}} = 5$ ns. As the up-conversion data shows, the laser emission occurs after several picoseconds and thus appears sufficiently earlier than the spontaneous emission. Again, the simulated time-resolved intensities using the rate equations (Fig. 4 (b)) is in good agreement with the experimental data.

Metal Layers: Tamm-Plasmon-Polaritons. In order to realize optoelectronic devices, electrical contacts are needed. In case of OLEDs, In₂O₃:Sn (ITO) with typical layer thicknesses of 80-150 nm is most commonly used as semitransparent electrode. The second way to efficiently contact an organic active layer is the utilization of thin metallic layers, which can easily be deposited by means of thermal evaporation under high vacuum. This fact motivates the

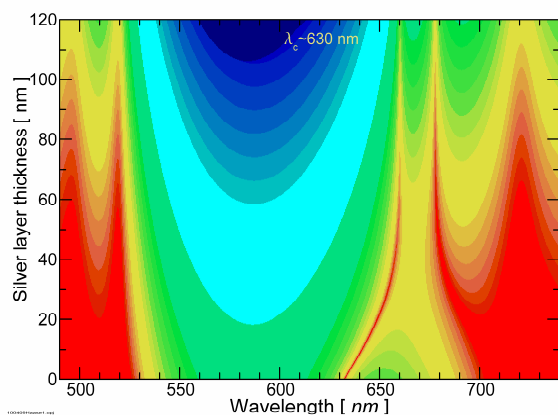


Fig. 5. Calculated transmission spectra of the organic MC with different thicknesses of Ag layer inserted between organic cavity layer and TiO₂ top layer of the bottom DBR.

This journal is © The Royal Society of Chemistry 2013

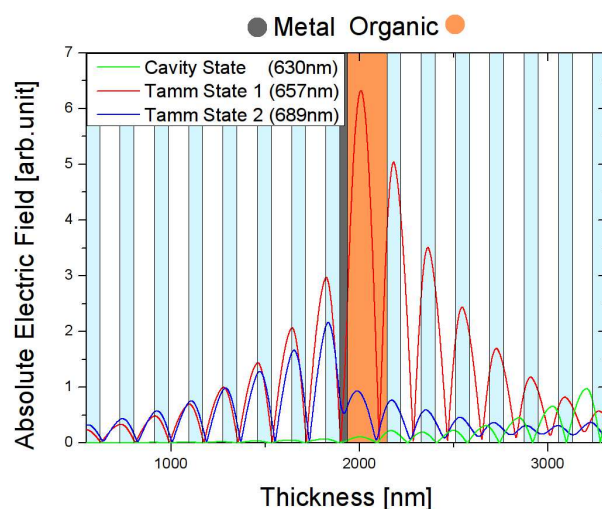


Fig. 6. Spatial distribution of the cavity modes with their wavelength 630, 657, and 686 nm in MC with inserted 40 nm silver layer between left DBR and organic layer.

study of metallic structures inside organic MCs which may enable electrical contacting. In addition, metals also may serve as broadband high-reflectivity mirrors and act as heat sink due to the high thermal conductivity²³.

Similar to electronic Tamm states at the surface of a crystal, optical Tamm states can form at the interface between two photonic structures having overlapping band gaps²⁴. The complex interplay between a metal layer and a periodic DBR results in the formation of localized surface states at the interface.

In order to verify this interpretation, the transfer matrix formalism²⁵ is utilized to numerically determine the transmission properties of a half-wavelength organic microcavity with included silver layer of increasing thickness (Fig. 5). At zero

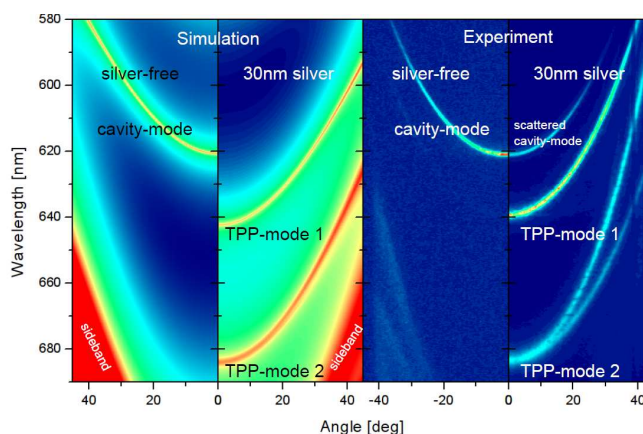


Fig. 7. Calculated (left panel) and experimental (right panel) angular-resolved transmission spectra without (left part) and with inserted 30 nm Ag layer.

J. Name., 2013, **00**, 1-3 | 4

ARTICLE

silver thickness, only one cavity resonance (TS1) exists at the design wavelength $\lambda_c = 632$ nm. Upon increasing the silver thickness up to ~ 40 nm, we observe a continuous shift of the cavity resonance towards lower energies and the emergence of a new mode (TS2) from the DBR side band shifting to higher energies. Both spectral movements of the modes saturate at a silver thickness of ~ 40 – 50 nm, at a minimal spectral distance of 22 nm. In Fig. 6, the simulated spatial distribution of the resonance cavity mode at $\lambda_c \sim 620$ nm demonstrates a substantial enhancement of the electric field in the cavity resulting in enhancement of the spontaneous emission.

In Fig. 7, the calculated and experimental transmission spectra of unpolarized light are presented. The simulated parameters are selected to obtain the best coincidence between experimental results and simulations for two cases without and with the embedded metallic layer. When metal is present, both Tamm states are visible, with the base eigenenergy of TS1 at 640 nm. This state is therefore supported by the gain of DCM and may preferentially show lasing. With no metal inside the structure, the ordinary cavity state is located at 620 nm.

To demonstrate and investigate experimentally the lasing from the Tamm-plasmon states, nanosecond pulses of 532 nm wavelength are utilized to pump neighboring regions either with or without 40 nm Ag layer. In this experiment, regions with homogeneous metal, 15 μm away from metal-free regions, are pumped via the focused beam (diameter of 3 μm). In Fig. 8, the angle-resolved emission patterns of the cavity in dependence on the excitation energy are presented. In panel (a), both the cavity state and the TS1 appear.

Examining the quality factor $Q = \lambda_c / \Delta\lambda_c$ of the modes leads to values of ~ 1400 for the cavity state and about ~ 650 for TS1. In

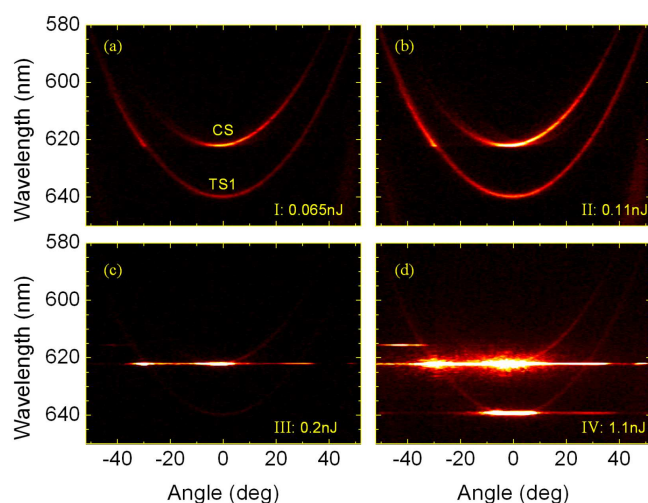


Fig. 8. Angular dispersion of the CS and TS1 in dependence on the excitation energy. (a) At low excitation energy, both modes are apparent with different intensities. (b) Increasing the pump energy leads to linearly increased spontaneous emission until (c), the threshold of the cavity mode is reached. (d) By further increasing the excitation, the emission of the TS1 mode at $k=0$ increases super-linearly indicating lasing.

This journal is © The Royal Society of Chemistry 2013

panel (b), the emission intensity is increased by a factor of two to 0.11 nJ. By further increasing the excitation energy, the coherence threshold of the cavity state is reached at 620 nm (panel (c), excitation energy 0.2 nJ). At $k = 0$ of the corresponding parabola, a super-linear increase in emission intensity is observed accompanied by a reduction in linewidth. A further increase in pump energy leads to the observation of a second non-linear threshold, this time of the TS1 at ~ 640 nm. A significant reduction of the spectral emission wavelength is a further evidence of lasing from a Tamm plasmon polariton, see panel (d).

Confined modes

Elliptic Holes in Metal Layer. Light propagating in 3D space is reflected from the interface between two media with different refractive indices n , or with different propagation constant β for a 2D waveguide. In a planar MC, light can be confined in the z direction between two DBRs, and additionally in elliptic islands in the xy space within the thin metal layers.

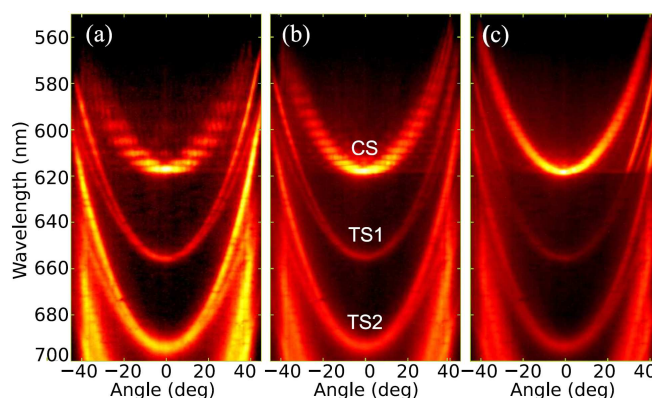


Fig. 9. Angle-resolved photoluminescence spectra of the metal-organic MC excited centrally in three holes of (a) 4 μm , (b) 7 μm , and (c) 10 μm diameter by a 405 nm cw laser beam with a 2- μm -diameter spot.

The far field emission of holes with different diameter (4, 7, and 10 μm) excited exactly in the middle of the hole is shown in Fig. 9 (a)-(c). The parabola-shaped dispersion curves with cutoff wavelengths at 655 nm (TS1) and 690 nm (TS2) originate from Tamm states formed due to the incorporated 40 nm silver layer. Each of the states is represented by a set of two parabolas as a result of the splitting between TE and TM polarized light at nonzero angles.

In addition to the states TS1 and TS2, a parabola-shaped discretized cavity state (CS) is present at 619 nm. The coexistence of Tamm states and the cavity parabola is explained by the lateral extent of the wave functions which may substantially overlap at regions next to the metal edge. The discrete far field pattern of the CS is a typical fingerprint of

ARTICLE

confined optical systems which is caused by the boundary conditions of the holes in the metal layer.²⁶

As expected for good optical confinement, the energy spacing between adjacent discrete levels decreases and the angular linewidth narrows when the hole diameter is increased (Fig. 9 (b)).²⁷⁻²⁸ With a further growing diameter, the energy splitting vanishes (Fig. 9 (c)) and the parabola narrows until, at about 15 μm hole diameter, it becomes indistinguishable from the delocalized cavity mode.

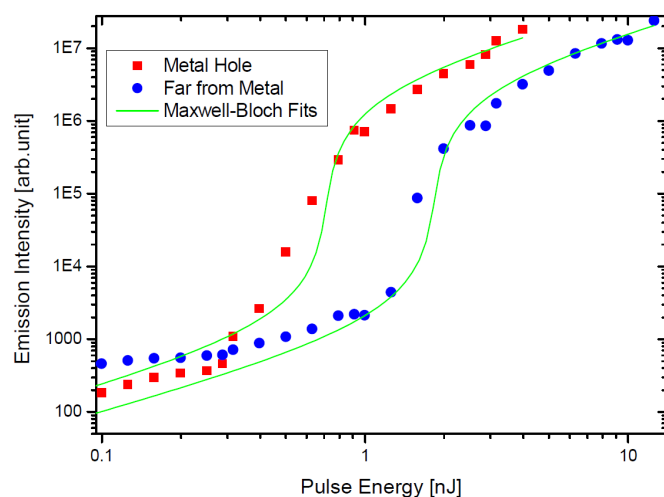


Fig. 10. Cavity state (squares) lasing threshold of 12 μm hole compared to unstructured spot (circles) confinement improves lasing threshold by decreasing cavity decay rate by factor of 3.

As presented in Fig. 10, lasing threshold and efficiency of the emission from μ -holes are improved in comparison to surrounded Tamm-plasmon-polariton states.

External Efficiency Control via Gain Spectrum and Periodic Structuring. Lai et al.²⁹ investigated emission from the array of periodically spaced metal stripes and observed coherent emission from both zero-ground state and Bloch-like excited π -states. In the following publications³⁰⁻³¹, it was shown that at higher excitations

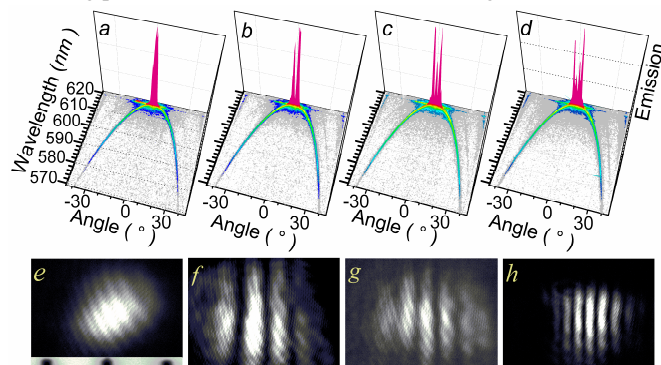


Fig. 11. Coherent multi-beam laser emission from organic planar MC at above-threshold periodically-modulated excitations with four different angles between two interfering excitation beams.

the extended and confined modes can simultaneously coexist and be manipulated optically, depending on the excitation spot position in periodically modulated inorganic MC structures. These coherent phenomena in photonic boxes and wires have been described theoretically.³²

Periodic distribution of gain in planar MCs can be created by two or more interfering laser beams with few-micron period depending on the angle between the excitation beams. In these cases, coherent emissions have a periodic distribution, resulting in two or more normal and oblique lasing beams.

In Fig. 11 (a-d), the coherent multi-beam laser emission from organic planar MCs at above-threshold periodically-modulated excitations is shown for four different angles between two interfering excitation beams. In addition to spontaneous emission with parabola-like dispersion (green), substantially strong multi-beam lasing emission peaks (pink) occur near the bottom of the parabola at $\theta = 0^\circ$. The corresponding spatial distributions of the emission patterns are presented in Fig. 11 (e-h).

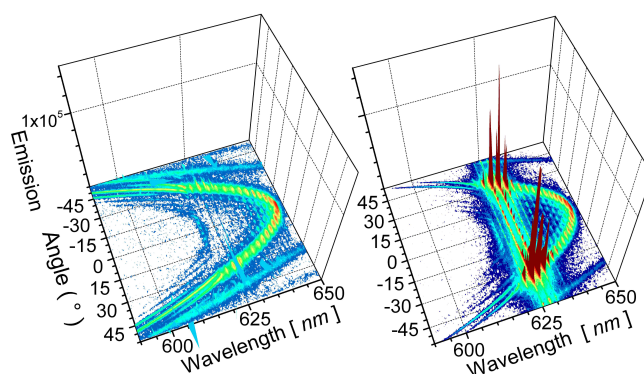


Fig. 12. Experimental angular-resolved emission spectra from organic MC with periodically-modulated cavity layer below (left) and above (right) lasing threshold.

In case of a periodically rectangular patterned cavity layer of the organic MC with periods ~ 7 and 11 μm , coincidence of extended and confined modes were observed in far-field emission spectra (Fig. 12).

Organic Light-Emitting Diodes

To achieve high luminous efficacy, the driving voltage of the OLED needs to be low. With the introduction of doped transport layers and exciton blocking layers, pin-OLEDs achieve driving voltages close to the thermodynamic limit. We will thus not further discuss this aspect here. In the following, the key factors which determine the external quantum efficiency (EQE) of OLEDs will be described and explained.

ARTICLE

External Quantum Efficiency^{33,34}. Regarding the electrical excitation, creation of electron-hole pairs and excitons, their radiative emission, and optical outcoupling processes, the external quantum efficiency η_{EQE} is defined as the ratio of the number of photons emitted from the device to the number of carriers injected into the molecular layers. It can split into four terms:

$$\eta_{\text{EQE}} = \gamma \eta_{\text{S/T}} \eta_{\text{r}} \eta_{\text{out}} \quad (6)$$

where γ is the electrical efficiency (also known as charge carrier balance factor). It describes the ratio of generated excitons to the number of injected electrons. The ratio of singlets/triplets is described by the exciton spin factor $\eta_{\text{S/T}}$, with $\eta_{\text{S/T}} = 1$ for phosphorescent emitters, and $\eta_{\text{S/T}} = 0.25$ for fluorescent emitters. The effective radiative efficiency η_{r} (or internal quantum efficiency of the emitter) describes the number of generated photons to the number of generated excitons:

$$\eta_{\text{r}} = F \Gamma_{\text{r}} / (\Gamma_{\text{r}} + \Gamma_{\text{nr}}). \quad (7)$$

The Purcell¹⁴ factor F accounts for the quantum mechanical effect that the radiative efficiency of an emitter depends on its surrounding. In free space $F = 1$, while in OLEDs, F ranges values below and above 1. Γ_{r} and Γ_{nr} are the radiative and nonradiative decay rates of the emitter, which are strongly dependent on the emission spectrum. Here, the wavelength dependency of the respective efficiencies (i.e. the photoluminescence, absorption and gain spectra) needs to be considered. Often, the product of the charge balance, the exciton spin factor, and the efficiency of radiative decay are summarized as the internal quantum efficiency $\eta_{\text{i}} \leq 1$.

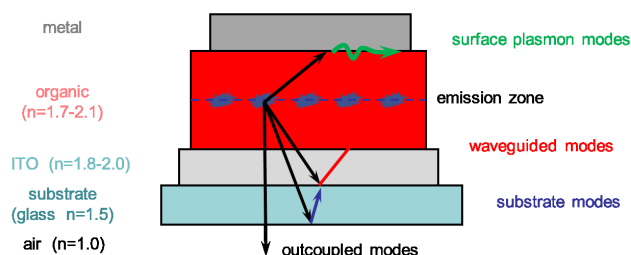


Fig. 13. Light loss mechanisms inside the OLED resulting from total internal reflection. The light modes can be distinguished into outcoupled, wave-guided, and surface plasmon modes. Absorption losses in the ITO and the doped transport layers can be expected to play a minor role. Refraction at the interfaces has been omitted for simplification.

Light Outcoupling. The last term in Eq. (6) is the outcoupling efficiency η_{out} . It accounts for the ratio of outcoupled photons to generated photons, i.e. the probability that light generated within the device is coupled out through the transparent substrate (Fig. 13). The outcoupling losses are caused by the different indices of

refraction of the organic materials, metal, ITO, and the glass substrate. Thus, reflected light will be trapped within the organic and the glass, which leads to absorption in the ITO and the metal cathode. As shown in Fig. 13, three different light modes can be distinguished within the device: (i) surface plasmon modes at the organic/metal interface, (ii) wave-guided modes, and (iii) substrate modes. These losses indicate that there is huge potential for efficiency improvement by outcoupling the trapped

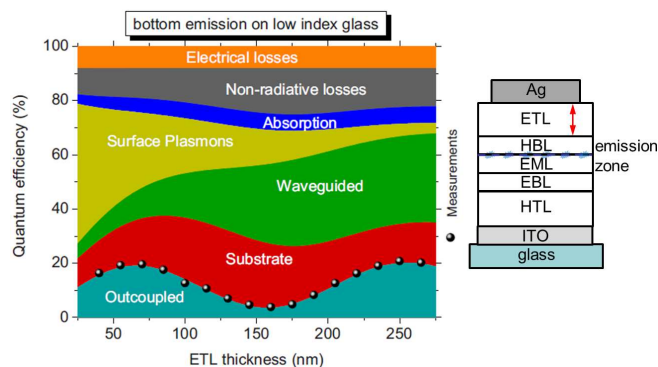


Fig. 14. Quantified loss mechanisms in a red phosphorescent pin-OLED for different ETL thicknesses by Meerheim et al.[34]. The simulated external quantum efficiency agrees nicely with experimental results (at low current density of 1.51 mA/cm², configuration as shown on the right side). Reprint with permission from [37]. Copyright 2010, American Institute of Physics.

modes.^{35,36}

The outcoupled emission exhibits a strong dependence on the EML position and thickness. Figure 14 shows the experimentally obtained EQE (dots) in conjunction with the simulated loss mechanisms for a red phosphorescent OLED. The outcoupled emission is characterized by a first maximum, a first minimum, and a second maximum. This can be understood by regarding the resonance condition inside the OLED cavity for 0°: $2L = m\lambda$, with $L = n_{\text{c}}d$ the optical thickness of the cavity (i.e. the cavity length d multiplied by the refractive index n_{c}) and $m = 1, 2, \dots$ the resonance order. The cavity condition is a result of constructive and destructive interference of the light modes. The calculation of the electromagnetic field confirms this condition. The calculated field intensity for different cavity lengths L and emitter positions is shown in Fig. 15.

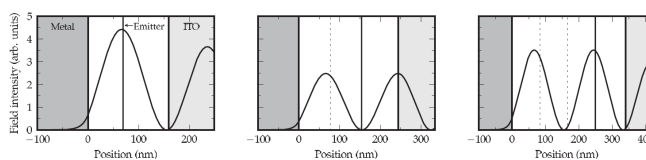


Fig. 15. Electromagnetic field intensities of the waveguide modes for the devices shown in Fig. 14 at the peak wavelength of the emitter (610 nm, 0°) for metal/organic/ITO structures. From left to right: 3/4 λ cavity with emitter located 70 nm from the metallic contact, 5/4 λ cavity with emitter at 155 nm, 5/4 λ cavity with emitter at 250 nm. Increasing the ETL thickness and thus the cavity thickness shifts the emitting molecules through a first maximum, a minimum, and a second maximum. Reprint with permission from [9]. Copyright 2010, American Institute of Physics.

ARTICLE

If the emitting molecules are placed in the maximum of the electromagnetic field, a large number of radiation modes are available, and therefore a strong coupling to the outcoupled modes can be expected. The coupling of the emitting molecules to the electromagnetic field influences the outcoupling efficiency strongly and explains qualitatively the dependence of the outcoupling efficiency in Fig. 14. Placing the emitters into the node of the field, in contrast, leads to low outcoupling efficiencies. The influence of the emitter coupling to the field and the Purcell effect on the outcoupling efficiency are often referred to as cavity effects.

A large number of methods have been studied to improve light outcoupling, for example, the use of a resonant cavity,³⁸ the excitation of surface plasmons³⁹, the use of periodic structures placed in the optically active layer to introduce Bragg scattering normal to the substrate plane⁴⁰, high refractive index glass in combination with a half-sphere⁴¹, and many more. Despite the fact that white OLEDs with fluorescent tube efficiencies can be achieved at lab scale, outcoupling methods for OLED fabrication on industrial scale are still pending.

Top-Emitting OLEDs

Top-emitting OLEDs are characterized by a highly reflective bottom electrode and a semitransparent top electrode, and in contrast to the previously described bottom-emitting OLEDs emit light away from the substrate. Thus, the OLED forms an MC, where the light is reflected back and forth between both electrodes leading to a narrowing of the emitted spectrum and inefficient light outcoupling at non-resonant conditions.

Capping Layer. To improve light outcoupling and to weaken the microcavity effects, a capping layer of a high-index material is deposited onto the top electrode. This changes the transmittance of top contact as known from thin film optics and improves the EQE of the OLED.⁴² In Fig. 16, it is demonstrated that the maximum efficiency is obtained at neither the highest nor the lowest

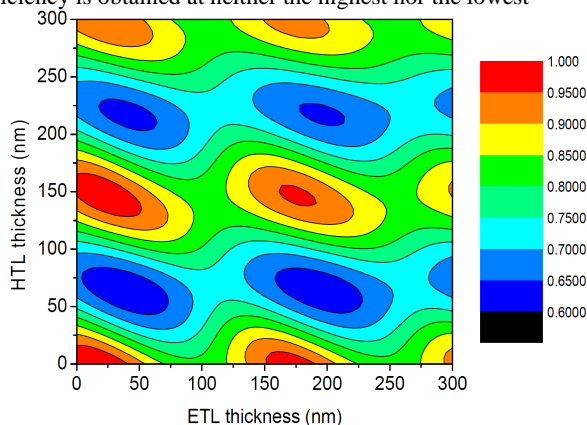


Fig. 16. Normalized light transmission of the top contact including the capping layer at the wavelength of 510 nm as a function of capping and spacer 1 layer thickness calculated based on the following OLED structure: Ag (80 nm)/spacer 1 (Y nm)/emitter (15 nm)/ spacer 2 (35 nm)/Ag (15 nm)/capping layer (X nm). The refractive index of all organic materials used is assumed to be 1.75.

transparency of the top contact, but at a certain value in between, which depends on the interference effects within the device.

In fact best outcoupling results are obtained when not only the transmittance of the top electrode is optimized by varying the capping layer, but when the optical structure of the whole device is adjusted.

Bragg Scattering⁴³⁻⁴⁷. In Fig. 17(a,b), angular-resolved *s*- and *p*-polarized spontaneous emission spectra of a planar top-emitting OLED are shown. As typical for MCs, the emitted light demonstrates parabolic angular dependence of emission spectra. In order to enhance the EQE, a corrugation in form of a line grating with 750 nm period and 40 nm height is introduced by a nano-imprint photoresist layer beneath the bottom electrode.

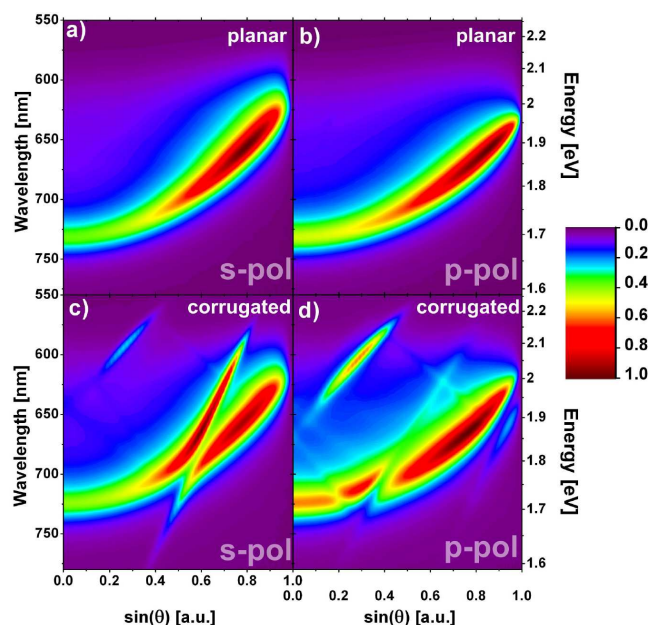


Fig. 17. Measured angular dependent emission spectra for *s*- and *p*-polarized light of planar (a-b) and corrugated top-emitting OLED (c-d) operating in the second optical maximum. Bragg scattering at the one dimensional shallow sub- μm grating superimposes sharp spectral features to the resonant cavity emission, resulting from constructive and destructive interference of the cavity emission and Bragg scattered modes. Reproduced from Ref. [46]. Copyright 2013, International Society for Optics and Photonics.

The corresponding emission spectra are given in Fig. 17(c,d). The Bragg scattering at the 1D grating superimposes sharp spectral features to the cavity-mode. By analyzing the measured emission spectra with the simulated emission for the whole *k* space, these features can be identified as Bragg scattered waveguided and surface plasmon modes of different orders (Fig. 18).

Moreover, the EQE of the corrugated OLED is enhanced by a factor of 1.16 in comparison to the planar reference.

ARTICLE

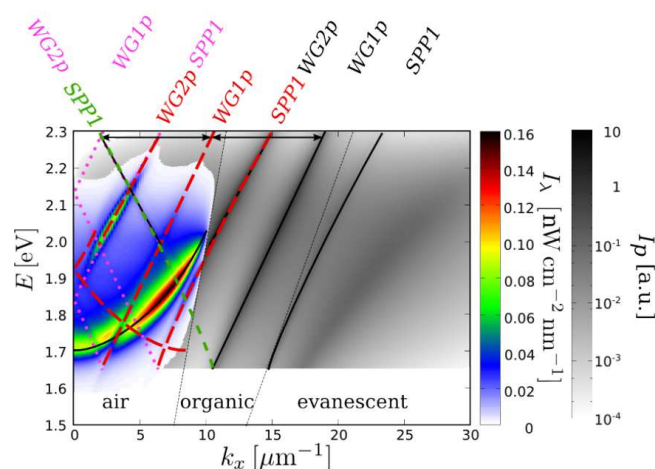


Fig. 18. Measured spectral radiant intensity of the corrugated device in p-polarization (false color scale) along with the simulated power dissipation spectra of the identical planar reference (gray-scale) outside the experimentally accessible region. Black arrows indicate the reciprocal lattice vector and link the modes of the simulated planar MC to the measured modes arising from Bragg scattering (colored lines: scattered surface plasmon (SPP) or wave-guided (WG) modes). Reproduced from Ref. [48]. Copyright 2013, International Society for Optics and Photonics.

Conclusions

The external efficiency of light-emitting structures is strongly influenced by their optical design. Our article discusses some approaches to increase the external efficiency of organic microcavities and organic light-emitting devices. In organic microcavities with high Q -factor ~ 1000 , where the emitting layer embedded by distributed Bragg reflectors, the 1D confinement increases spontaneous emission due to Purcell effect. Further optimization of thicknesses of the metal, active organic and adjusting dielectric layer minimizes absorption of light by metal, allowing the lasing of the coupled Tamm-plasmon polaritons. High above threshold excitation, lasing substantially increases the ratio between radiative and non-radiative emission. Corrugation of metal contacts, like perforated μ -size holes or periodic array of metal stripes leads to 2D confinement of cavity modes, decreasing the lasing threshold.

Using light refractive, diffractive, or scattering elements in OLEDs, the external quantum efficiency can be strongly enhanced. Especially for top-emitting OLEDs a dielectric organic capping layer and periodically structured line-grating increase the efficiency. It is expected that by optimization of the grating period, grating height, and the implementation of two-dimensional gratings, the light outcoupling and thus the EQE can be further improved.

Acknowledgements

We thank Mauro Furno, Qiang Huang, Rico Meerheim, Tobias Schwab, Cornelius Fuchs, Robert Brueckner, Andreas Mischok, and Markas Sudzius. The authors gratefully acknowledge the financial support of this work by the Bundesministerium für Bildung und Forschung (BMBF), Deutsche Forschungsgemeinschaft (also via the excellence cluster CfAED), and the European Community.

Notes and references

^a Institut für Angewandte Photophysik, TU Dresden, 01069 Dresden, Germany

* E-mail: karl.leo@iapp.de

- 1 R. Brückner, A.A. Zakhidov, R. Scholz, M. Sudzius, S. I. Hintschich, H. Fröb, V. G. Lyssenko and K. Leo, *Nature Photonics* 2012, **6**, 322
- 2 C. W. Tang and S. A. Van Slyke, *Appl. Phys. Lett.*, 1987, **51**, 913.
- 3 J. Blochwitz, M. Pfeiffer, T. Fritz and K. Leo, *Appl. Phys. Lett.* 1998, **73**, 729.
- 4 M. Pfeiffer, T. Fritz, J. Blochwitz, A. Nollau, B. Plönnigs, A. Beyer and K. Leo, *Advanc. in Solid State Phys.*, 1998, **39**, 77.
- 5 J. Blochwitz. "Organic light-emitting diodes with doped charge transport layers". TU Dresden (Dissertation), 2001.
- 6 J. Huang, M. Pfeiffer, A. Werner, J. Blochwitz, K. Leo and S. Liu. *Appl. Phys. Lett.*, 2002, **80**, 139.
- 7 M. Pfeiffer, K. Leo, X. Zhou, J. S. Huang, M. Hofmann, A. Werner and J. Blochwitz-Nimoth, *Organic Electronics*, 2003, **4**, 89.
- 8 W.L. Barnes, A. Dereux, and T.W. Ebbesen, *Nature* 2003, 424, 824.
- 9 M. Furno, R. Meerheim, S. Hofmann, B. Lüsse and K. Leo, *Phys. Rev. B*, 2012, **85**, 115205.
- 10 H. Benisty, H. De Neve, and C. Weisbuch, *IEEE J. Quantum Electron.*, 1998, **34**, 1632.
- 11 J. A. E. Wasey and W. L. Barnes, *J. Modern Optics*, 2000, **47**, 725.
- 12 S. Astilean and W. L. Barnes, *Appl. Phys. B*, 2002, **95**, 591.
- 13 Y. Rag Do, Y.-C. Kim, Y.-W. Song and Y.-H. Lee, *J. Appl. Phys.*, 2004, **96**, 7629.
- 14 B.C. Krummacher, J. Frischeisen, N.A. Reinke and W. Brütting, *J. Appl. Phys.*, 2008, **104**, 123109.
- 15 C. Weisbuch, M. Nishioka, A. Ishikawa and Y. Arakawa, *Phys. Rev. Lett.* 1992, **96**, 3314.
- 16 J. M. Gérard, B. Sermage, B. Gayral, B. Legrand, E. Costard and V. Thierry-Mieg, *Phys. Rev. Lett.* 1998, **81**, 1110.
- 17 E. M. Purcell, *Phys. Rev.* 1946, **69**, 681.
- 18 P.R. Rice and H.J. Carmichael, *Phys. Rev. A*, 1994, **50**, 4318.
- 19 G. Bjork and Y. Yamamoto, *IEEE J. Quantum Electron.*, 1991, **27**, 2386.
- 20 Y. Yamamoto, S. Machida, and G. Bjork, *Opt. Quantum Electron.* 1992, **24**, S215.

ARTICLE

- 21 H. Yokoyama and S. D. Brorson, *J. Appl. Phys.* 1988, **66**, 4801.
- 22 M. Koschorreck, R. Gehlhaar, V.G. Lyssenko, M. Swoboda, M. Hoffmann and K. Leo, *Appl. Phys. Lett.* 2005, **87**, 181108.
- 23 C.-Y. Lu, S.-W. Chang, S. L. Chuang, T. D. Germann and D. Bimberg, *Appl. Phys. Lett.* 2010, **96**, 251101.
- 24 A. V. Kavokin, I. A. Shelykh and G. Malpuech. *Phys. Rev. B* 2005, **72**, 233102.
- 25 M. Kaliteevski, I. Iorsh, S. Brand, R. Abram, J. Chamberlain, A. Kavokin and I. Shelykh. *Phys. Rev. B* 2007, **76**, 165415.
- 26 M. Langner, M. Sudzius, H. Fröb, V. G. Lyssenko and K. Leo, *Appl. Phys. Lett.*, 2009 **95**, 091109.
- 27 A. Muller, C.-K. Shih, J. Ahn, D. Lu, D. Gazula and D. G. Deppe, *Appl. Phys. Lett.* 2006, **88**, 031107.
- 28 C. Reinhardt, R. Brückner, J. Haase, M. Sudzius, S. I. Hintschich, H. Fröb, V. G. Lyssenko and K. Leo, *Appl. Phys. Lett.*, 2012, **100**, 103306.
- 29 C. W. Lai, N.Y. Kim, S. Utsunomiya, G. Roumpos, H. Deng, M. D. Fraser, T. Byrnes, P. Recher, N. Kumada, T. Fujisawa and Y. Yamamoto, *Nature (London)* 2007, **450**, 529.
- 30 E. Wertz, L. Ferrier, D. D. Solnyshkov, R. Johné, D. Sanvitto, A. Lemaître, I. Sagnes, R. Grousson, A. V. Kavokin, P. Senellart, G. Malpuech and J. Bloch, *Nature Phys.* 2010, **6**, 860.
- 31 L. Ferrier, E. Wertz, R. Johné, D.D. Solnyshkov, P. Senellart, I. Sagnes, A. Lemaître, G. Malpuech, and J. Bloch, *Phys. Rev. Lett.* 2011, **106**, 126401. .
- 32 M. Wouters, T.C.H. Liew and V. Savona, *Phys. Rev. B* 2010, **82**, 245315.
- 33 K. Walzer, B. Maennig, M. Pfeiffer and K. Leo, *Chem. Rev.*, 2007, **107**, 233.
- 34 R. Meerheim, B.Lüssem, and K.Leo, *Proceedings of the IEEE*, 2009, **97**, 1606.
- 35 L. Xiao, Z. Chen, B. Qu, J. Luo, S. Kong, Q. Gong and J. Kido. *Advanc. Materials* 2011, **23**, 926. .
- 36 G. He, M. Pfeiffer, K. Leo, M. Hofmann, J. Birnstock, R. Pudzich and J. Salbeck. *Appl. Phys. Lett.* , 2004, **85**, 3911.
- 37 R. Meerheim, M. Furno, S. Hofmann, B. Lüssem and K. Leo, *Appl. Phys. Lett.*, 2010, **97**, 253305.
- 38 T. Shiga, H. Fujikawa and Y. Taga, *J. Appl. Phys.*, 2003, **93**, 19.
- 39 P. Andrew and W. L. Barnes, *Science* 2004, **5**, 1002.
- 40 J. Feng, T. Okamoto and S.Kawata, *Appl. Phys. Lett.*, 2005, **87**, 241109.
- 41 J. M. Lupton, B.J. Matterson, I. D. W. Samuel, M. J. Jory, and W. L. Barnes, *Appl. Phys. Lett.*, 2000, **77**, 3340.
- 42 R. Reineke, F. Lindner, G. Schwartz, N. Seidler, K. Walzer, B. Lüssem, and K. Leo, *Nature* 2009, **459**, 234
- 43 Q. Huang, K. Walzer, M. Pfeiffer, K. Leo, M. Hofmann and T. Stübinger, *J. Appl. Phys.*, 2006, **100**, 064507.
- 44 P. A. Hobson, S. Wedge, J. A. E. Wasey, I. Sage, W. L. Barnes, *Advac. Materials*, 2002, **14**, 1393.
- 45 L. H. Smith, J. A. E. Wasey, I. D. W. Samuel, and W. L. Barnes, *Adv. Funct. Mater.*, 2005, **15**, 1839.
- 46 T. Schwab, C. Fuchs, R. Scholz, X.Li, F. Xie, W. Choy, K. Leo, and M.C. Gather, *Proc. of SPIE* 2013, 882911
- 47 T. Schwab, C. Fuchs, R. Scholz, A. Zakhidov, K. Leo, and M. C. Gather, *Opt. Express* 2014, **22**, 7524
- 48 C. Fuchs, T. Schwab, T. Roch, S. Eckard, A. Lasagni, S. Hofmann, B. Lüssem, L. Müller-Meskamp, K. Leo, M.C. Gather, and R. Scholz, *Opt. Express* 2013, **21**, 16319.